Excited electron dynamics in Cu nanowires supported on a Cu(111) surface

Sergio Díaz-Tendero,[1,2] Fredrik E. Olsson,[3] Andrey G. Borisov,[1,2] and Jean-Pierre Gauyacq[1,2,*]
[1]*CNRS, Laboratoire des Collisions Atomiques et Moléculaires, UMR 8625, Bâtiment 351, Universite Paris-Sud, 91405 Orsay Cedex, France*
[2]*Université Paris-Sud, Laboratoire des Collisions Atomiques et Moléculaires, UMR 8625, Bâtiment 351, Université Paris-Sud, 91405 Orsay Cedex, France*
[3]*Department of Applied Physics, Chalmers/Göteborg University, S-41296 Göteborg, Sweden*
(Received 24 November 2008; revised manuscript received 21 January 2009; published 26 March 2009)

We present a theoretical study of the excited electron dynamics in infinite Cu monoatomic chains (nanowires) supported on a Cu(111) surface. A joint approach based on the wave packet propagation and the density functional theory is used. The nanowire-induced potential obtained from *ab initio* density functional theory calculations serves as an input for the wave-packet propagation study of the excited electron dynamics. The energy dispersion and the lifetime of an unoccupied one-dimensional (1D) nanowire-localized electronic band with *sp* character are obtained. From the group velocity and lifetime of the 1D *sp*-band states, it follows that an excited electron can travel about four to five atomic sites along the nanowire before its escape into the bulk. We show that the surface projected band gap and the surface Brillouin zone backfolding of the substrate states play a fundamental role in the lifetime of the nanowire-localized states.

DOI: 10.1103/PhysRevB.79.115438 PACS number(s): 73.20.At, 73.20.Hb, 73.21.Hb, 73.63.Nm

I. INTRODUCTION

Artificial nanostructures at surfaces resulting either from self-organization of adsorbed species[1–3] or atom-by-atom building with scanning tunneling microscope (STM) manipulation[4–6] attract considerable interest from both fundamental and practical points of view. Indeed, studies of quantum corrals[7–15] and quantum mirages[10,14,16–18] showed that nonmagnetic and magnetic nanostructures can be built with tailored electronic properties. In the above examples, the underlying physics consists in the quantization of the two-dimensional (2D) continuum of the intrinsic surface state by the corral structure.[7,8] Similarly, electron confinement of 2D surface state, image potential states, and quantum well continua has been also observed in adatom and vacancy islands,[19–26] and in terraces bounded by steps.[27–30] Along with modification of the substrate states, artificial nanostructures can lead to the appearance of new electronic states such as has been observed for the monoatomic chains at surfaces—subject of the present theoretical study.

Metal monoatomic chains were built recently with STM manipulation at various substrates.[31–40] The atom-by-atom construction of the chain allowed to follow the evolution of its electronic properties with the chain length and link them to the electronic properties of a single metal adatom. Thus, Cu adatoms on Cu(111) surface and similarly Au and Pd adatoms on NiAl(110) surface induce an adatom localized resonance in the electronic density of states above the Fermi level and inside the surface projected band gap of the substrate. The latter characteristic is of central importance, as explained below. As shown by *ab initio* studies,[34,41–43] an adatom-localized resonance is formed by the hybridization of the *sp* adatom orbitals. When the adatoms are aligned into a chain, the *sp* resonances located at neighboring sites are coupled. For an infinite chain (called a "wire" below), a one-dimensional (1D) *sp*-band of excited electronic states appears. For a finite-size chain, the excited electronic states correspond to the quantization of the 1D *sp*-band by the chain boundaries. This is supported by the comparison between an *ab initio* studies[34,41,43] and experimental data, as well as by the successful description of the experiment by simple models based on the above picture.[31,32,38,39] Recently, it was also shown that in the case of a circular closed line of Cu adatoms (a circular corral) on Cu(111), an excited *sp* resonance appears delocalized on the curved line of adatoms; the presence of this excited state was shown to significantly alter the energy spectrum and the lifetime of the surface state confined inside the corral.[44]

In the case of a straight atomic line, an excited electron injected into the 1D *sp*-band would propagate along the atomic chain for some distance before it vanishes into the substrate. Obviously, this system is a surface-supported analog of the freestanding nanowires or of the nanowires connecting metal leads thoroughly studied over the last years[45–49] because of their possible applications in nanoscale electronics[50] as well as the possibility of using them as gas sensors.[51] For any system thought to serve as a wire for nanoelectronic applications, the ability to support an electron flux is crucial. While for freestanding nanowires or nanowires connecting metal leads the major phenomena controlling the electronic properties and conductivity are quite well understood,[50,52–54] metal supported monoatomic chains have been mostly studied only from the point of view of the energies of their electronic states.[34,38,41,55] It has been shown that the dispersion of the 1D *sp*-band can be well described with a tight-binding (TB) modeling *only* including the electronic states localized on the chain atoms.[34,35,38,41] This is a remarkable result since, for e.g., a Cu atom in the Cu wire supported on the Cu(111) surface, one expects similar couplings with its two neighbors in the wire and with its three nearest neighbors in the substrate. (We assume fcc adsorption sites for the chain atoms.[34]) Thus, instead of propagating along the wire, an electron would rather escape into the substrate. It has been argued that owing to the projected band gap of the substrate, the nanowire-localized states are partly

decoupled from the substrate which directly affects their lifetimes.[32,41] Indeed, excited states at metal surfaces decay via energy-conserving one-electron transfer into the continuum of the electron states of the substrate and via many-body energy relaxation.[56] Decoupling from the continuum of the electronic states of the metal *a priori* should increase the lifetime of the nanowire-localized states, as was reported for the alkali adsorbate induced resonances on the (111) surfaces of noble metals.[57–61] The detailed study of the lifetimes of the nanowire-localized states appears timely, since the lifetime determines how long an excited electron can propagate along the nanowire, i.e., whether an atomic wire on a metal surface can be considered as an almost independent entity, or simply as a protruding part of the substrate.

In a recent work,[62] we have studied the energy and lifetime of the excited 1D *sp*-band of the electronic states localized on a monoatomic Cu wire supported on the Cu(111) surface. Scanning tunneling spectroscopy (STS) data have been compared with theoretical calculations for electron momenta along the wire k_z up to 0.4 a.u. Supported by the good agreement with experimental data, the calculations could unravel the role of the surface-projected band gap of Cu(111) in (partially) decoupling the nanowire from the substrate, and thus stabilizing the nanowire-localized states. As a result of the projected band-gap effect, we found that an electron injected into the *sp*-band can travel a distance up to 12 Å before it escapes from the nanowire into the substrate.

The present contribution extends the study of Ref. 62 in several aspects. (i) The energy dispersion and the lifetime of the 1D *sp*-band of the Cu-wire/Cu(111) system is computed in a broad range of k_z. This allows to reach the regime where the surface Brillouin zone backfolding leads to a dramatic increase in the energy-conserving resonant electron transfer rate from the 1D *sp*-band into the electronic states of the substrate. Correspondingly, the lifetime of the 1D *sp*-band states decreases. [See Ref. 63 for a similar effect in the case of the 2D quantum well states in $p(2\times2)$ Cs and Na ordered overlayers on Cu(111).] (ii) The different decay paths of the nanowire-localized states are analyzed. It is shown that the electron escapes from the nanowire into both the 3D continuum of the propagating bulk states and the 2D continuum of the Cu(111) Shockley surface state. The surface state is the dominating decay channel for low k_z values when the 1D *sp*-band of nanowire localized states is outside the backfolded bulk continuum. (iii) Finally, a detailed account of the theoretical methods and approaches used in the calculation of the nanowire-localized states is presented.

The paper is organized as follows. In Sec. II the theoretical approaches are detailed. Section III presents the results, their discussion and comparison with recent experimental data. We end with some conclusions in Sec. IV. Throughout the paper, atomic units are used in equations, unless otherwise stated.

II. THEORETICAL METHODS

The system under study is schematically represented in Fig. 1. The Cu adatoms occupy the fcc adsorption sites on a Cu(111) surface and form an infinite monoatomic wire structure. The nanowire is along one of the ⟨110⟩ directions of the surface with the nearest-neighbor distance of $L=a/\sqrt{2}=2.55$ Å between Cu adatoms in the wire ($a=3.59$ Å is the lattice constant of Cu). With the above geometry, the present system is an infinite analog of the finite-size Cu chains studied experimentally by STM and STS.[34,35] The distance between the Cu nanowire and the last layer of surface atoms is 1.92 Å, as obtained here.

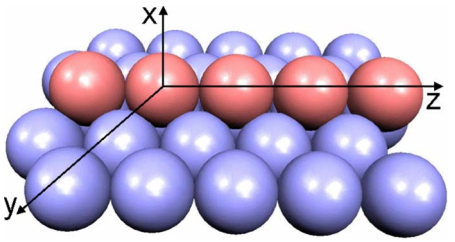

FIG. 1. (Color online) Schematic representation of a Cu nanowire supported on a Cu(111) surface. The Cu atoms in the wire are adsorbed in fcc sites of the surface and along one of the ⟨110⟩ directions. For the sake of clarity, the Cu atoms forming the wire and the substrate Cu atoms appear in different colors (red and blue respectively in the online version).

The dynamics of an excited electron in the nanowire is studied within a one-electron wave packet propagation (WPP) approach. The potential in which the excited electron evolves is obtained via a mixed approach in which the nanowire-induced potential is obtained by *ab initio* density-functional theory (DFT) calculations and the Cu(111) surface is represented with a model potential.[64] A description of the WPP technique can be found in Refs. 56 and 65 and references therein. The method employed here for the construction of the total potential of the system is described in Refs. 42, 66, and 67. Thus, we limit the description below to the points specific to the present study.

A. Time propagation

The core of the WPP consists in the direct solution of the time-dependent Schrödinger equation for the wave function of the excited electron $\Psi(\mathbf{r},t)$ represented on a 3D mesh in Cartesian coordinates $\mathbf{r}=(x,y,z)$. The z axis is chosen along the wire, and the x axis is normal to the surface and goes through the center of the Cu-wire atom placed at the coordinate origin (see Fig. 1). The system is periodic along the wire (z coordinate) so that $\Psi(\mathbf{r},t)$ can be represented in a Bloch form:

$$\Psi(\mathbf{r},t) = e^{ik_z z}\psi_{k_z}(\mathbf{r},t), \tag{1}$$

with

$$\psi_{k_z}(x,y,z+L,t) = \psi_{k_z}(x,y,z,t). \tag{2}$$

The time evolution of $\psi_{k_z}(\mathbf{r},t)$ is governed by the Hamiltonian H_{k_z}:

$$i\frac{\partial\psi_{k_z}(\mathbf{r},t)}{\partial t} = H_{k_z}\psi_{k_z}(\mathbf{r},t), \tag{3}$$

where

$$H_{k_z} = \underbrace{-\frac{1}{2}\left[\frac{\partial^2}{\partial x^2} + \frac{\partial^2}{\partial y^2} + \left(\frac{\partial}{\partial z} + ik_z\right)^2\right]}_{T_{k_z}} + V(\mathbf{r}). \tag{4}$$

T_{k_z} is the "effective" kinetic energy operator. $V(\mathbf{r})$ is the total potential acting on the electron. It is given by

$$V(x,y,z) = V_S(x) + V_W(x,y,z) + V_{\mathrm{Abs}}(x,y), \tag{5}$$

where $V_S(x)$ is the model electron-surface interaction potential proposed by Chulkov *et al.*[64] This potential depends only on the electron coordinate x perpendicular to the surface and correctly reproduces the main physical features of the Cu(111) surface at the $\bar{\Gamma}$ point: the projected band gap between −5.83 eV and −0.69 eV (all energies are measured with respect to the vacuum level), Shockley-type surface state at −5.27 eV, first image potential state at −0.82 eV. $V_W(x,y,z)$ is the nanowire-induced potential obtained from the *ab initio* DFT calculations described below. $V_{\mathrm{Abs}}(x,y)$ is an absorbing potential.[68] Placed at the x boundary of the computational mesh deep inside the metal and at both y boundaries, $V_{\mathrm{Abs}}(x,y)$ imposes the outgoing wave boundary conditions consistent with the search for the nanowire-localized quasistationary states.

Provided an initial condition $\psi_{k_z}(\mathbf{r},t=0)=\psi_0(\mathbf{r})$, the time evolution is obtained by numerical short time propagation with a typical propagation time step $\Delta t=0.05$ a.u. The "split-operator" technique[69,70] is used:

$$\psi_{k_z}(\mathbf{r},t+\Delta t) = e^{-iV\Delta t/2} e^{-iT_{k_z}\Delta t} e^{-iV\Delta t/2} \psi_{k_z}(\mathbf{r},t). \tag{6}$$

The action of the $e^{-iV\Delta t/2}$ operator on the wave function is local. The action of the $e^{-iT_{k_z}\Delta t}$ operator is calculated with the Fourier grid pseudospectral method.[71,72]

The nanowire-localized quasistationary states appear as exponentially decaying resonances of the system. Their energies E and decay rates Γ can be extracted from $\sigma(\omega)$, the density of states projected on the initial state (PDOS),

$$\sigma(\omega) = \frac{1}{\pi}\mathrm{Re}\left\{\int_0^\infty e^{i(\omega+i\eta)t} A(t)dt\right\}_{\eta\to+0}, \tag{7}$$

where the survival amplitude, $A(t)$, is defined as

$$A(t) = \langle \psi_0(\mathbf{r}) | \psi_{k_z}(\mathbf{r},t)\rangle. \tag{8}$$

The resonances are associated with Lorentzian structures in $\sigma(\omega)$. Note that within the present one-electron picture the width of the resonance is equal to its decay rate. Once the resonance energy E is known, the corresponding wave function can be extracted from the WPP calculation through

$$\psi_E(\mathbf{r}) = \int_0^\infty e^{iEt}\Psi(\mathbf{r},t)dt. \tag{9}$$

The propagation time required to reach the convergence of the PDOS can be extremely long when long-lived states are present. In this case, E and Γ can be obtained via the direct fit of $A(t)$ to a sum of several exponentially decaying terms (see Ref. 56 for details).

Obviously, an appropriate choice of the initial wave packet $\psi_0(\mathbf{r})$ can considerably ease the extraction of the energies and widths of the quasistationary states. In this work we are interested in the quasistationary 1D *sp*-band of the Cu wire, which is formed by the hybridization of the *sp* orbitals located at the individual Cu atoms of the wire and is polarized perpendicular to the surface. Accordingly, we have performed WPP calculations with an initial wave packet given by

$$\psi_0(\mathbf{r}) = xe^{-(x^2+y^2+z^2)/b}, \tag{10}$$

i.e., mimicking the p_x orbital centered on the Cu atom of the wire. The parameter b was set equal to 12.5 a_0^2.

B. Nanowire-induced potential

The nanowire-induced potential V_W has been obtained from *ab initio* DFT studies of the clean Cu(111) surface and Cu-wire/Cu(111), in a methodology similar to the one carried out in Refs. 42, 66, and 67. For the DFT calculations, we used a plane-wave pseudopotential method as implemented in the VASP code.[73] For an efficient and straightforward generation of V_W in the wave packet propagation, we used a nonlocal norm-conserving pseudopotential V_{PP} of Kleinman-Bylander type[74] to describe electron-Cu core interactions. This potential has the general form

$$V_{\mathrm{PP}} = V_{\mathrm{loc}} + \sum_l |V_l\rangle\langle V_l|, \tag{11}$$

where V_{loc} is the local part and $|V_l\rangle$ is the nonlocal projector with angular momentum component l. The exchange and correlation interactions were treated within a local-density approximation (LDA).[75,76] The Cu surface was represented by a slab containing four Cu layers, a 8.3 Å vacuum region (in the direction perpendicular to the surface, x) and a 4×1 surface unit cell (y and z directions, respectively). The adsorption height of the Cu atom in an fcc hollow site on the Cu(111) face of the slab was optimized, whereas the surface atoms were fixed at their bare surface equilibrium positions. We obtained an adsorption distance of 1.92 Å between the nanowire and the surface layer of Cu atoms. Comparing the DFT calculations on the clean Cu(111) surface and on the atomic chain+Cu(111) systems, we extract various quantities induced by the presence of the Cu atomic chain. Note that the substrate atoms were not allowed to relax in the compound system to facilitate the computation of the wire-induced quantities.

With the density-functional inputs, the wire-induced potential V_W is calculated from the nonlocal part of the V_{PP} potential, the wire-induced Hartree potential V_H^{ind}, and the induced exchange-correlation potential $V_{\mathrm{xc}}^{\mathrm{ind}}$. Several steps are followed.

(1) The wire-induced total charge density ϱ^{ind} verifying the constraint of the charge neutrality is calculated as

$$\varrho^{\mathrm{ind}} = -[n_{\mathrm{wire}} - n_0] + \frac{1}{4\pi}\Delta V_{\mathrm{loc}}, \tag{12}$$

where n_{wire} and n_0 are the electron densities of the surface with a wire and the bare Cu(111) surface, respectively. Thus,

the term in the square brackets corresponds to the wire-induced electronic density. The last term is obtained via inversion of the Poisson equation (Δ is the Laplace operator). It represents the positive charge density responsible for the V_{loc} potential. Note that V_{loc} is the local part of the pseudopotential describing an electron interaction with the Cu atom in the wire. It is acting on the electron and so includes the negative electron charge.

(2) The wire-induced exchange-correlation potential $V_{\mathrm{xc}}^{\mathrm{ind}}$ is calculated as

$$V_{\mathrm{xc}}^{\mathrm{ind}} = V_{\mathrm{xc}}^{\mathrm{wire}} - V_{\mathrm{xc}}^{0}, \tag{13}$$

where $V_{\mathrm{xc}}^{\mathrm{wire}}$ and V_{xc}^{0} are the exchange-correlation potentials of the surface with a wire and of the bare Cu(111) surface, respectively.

(3) Both ϱ^{ind} and $V_{\mathrm{xc}}^{\mathrm{ind}}$ obtained from Eqs. (12) and (13) are well confined in x and y directions inside the DFT-calculation supercell and they are represented on the same grid of Cartesian coordinates as in the VASP code. The $V_{\mathrm{xc}}^{\mathrm{ind}}$ is then projected on a plane-wave basis allowing the direct interpolation on the Cartesian grid used in the wave packet propagation.

(4) The wire-induced Hartree potential V_H^{ind} is given by the Poisson equation with ϱ^{ind} as a source:

$$\Delta V_H^{\mathrm{ind}} = -4\pi\varrho^{\mathrm{ind}}. \tag{14}$$

Equation (14) is solved with a pseudospectral approach. Using the periodicity of the system in the z direction, Eq. (14) can be recast in the following form in cylindrical coordinates $\mathbf{r}=(\rho,\varphi,z)$:

$$\underbrace{\left[-\frac{\partial^2}{\partial\rho^2}+\frac{m^2}{\rho^2}+(j\mathcal{G})^2\right]}_{T_\rho} V_H^{\mathrm{ind}}(m,j\mathcal{G},\rho) = 4\pi\varrho^{\mathrm{ind}}(m,j\mathcal{G},\rho), \tag{15}$$

where m and j are integers, $\mathcal{G}=2\pi/L$ is the reciprocal lattice vector along the nanowire (L is the period). The expansion coefficients $V_H^{\mathrm{ind}}(m,j\mathcal{G},\rho)$ and $\varrho^{\mathrm{ind}}(m,j\mathcal{G},\rho)$ are defined as

$$V_H^{\mathrm{ind}}(\rho,\varphi,z) = \frac{1}{\sqrt{\rho}}\sum_{m,j} V_H^{\mathrm{ind}}(m,j\mathcal{G},\rho)e^{im\varphi}e^{ij\mathcal{G}z},$$

$$\varrho^{\mathrm{ind}}(\rho,\varphi,z) = \frac{1}{\sqrt{\rho}}\sum_{m,j} \varrho^{\mathrm{ind}}(m,j\mathcal{G},\rho)e^{im\varphi}e^{ij\mathcal{G}z}. \tag{16}$$

A three-point finite difference method with zero boundary conditions in ρ is used to obtain the matrix representation of the T_ρ operator[77] inside a cylinder with a radius of several hundreds atomic units. Equation (15) is then solved for each m and j, and V_H^{ind} is calculated on the WPP mesh from Eq. (16). It is worth mentioning that using the total induced charge density ϱ^{ind} keeps the calculation cell neutral, avoids the logarithmic divergence of the potential at large ρ, and allows an efficient implementation of the above procedure.

With all the above definitions, the wire-induced potential used in our WPP study has the form

$$V_W = V_{\mathrm{xc}}^{\mathrm{ind}} + V_H^{\mathrm{ind}} + \sum_l |V_l\rangle\langle V_l|. \tag{17}$$

Obtained in this way, V_H^{ind} and therefore V_W is free from artifacts due to the supercell periodicity of the DFT calculation, particularly in the y direction along the surface.

It is worth noting that the spatial grid used in the WPP is much larger than the supercell used in the DFT calculations. Thus, the band structure of the semi-infinite substrate can be fully accounted for. In addition, the WPP calculation of the energies and widths does not suffer from the quantization of the continuum states in the finite box, since the optical absorbing potential imposes the proper outgoing wave boundary conditions. The WPP calculation can then yield the lifetimes of the quasistationary states in the system. Typically the WPP grid covers the 3D box: $-149.875<x<41.875$ a.u. perpendicular to the surface, $-95.875<y<95.875$ a.u. parallel to the surface and perpendicular to the wire, and $-2.398<z<2.398$ a.u. along the wire (see Fig. 1). The optical absorbing potential occupies a 50 a.u. region at the negative x and both y extremities of the mesh. The uniform grid comprises $N_x=768\times N_y=768\times N_z=24$ points. With the periodicity introduced in the z direction we thus describe the problem of an infinite Cu wire. Systems with a finite number of Cu atoms such as dimers or trimers are out of the scope of the present work. Though, the present results of the infinite chain can be compared with experimental data of finite-size chains, obtained via the analysis of their electronic states in terms of confined states in the chain.[34]

The construction of the effective electron potential, as described above, superimposes a model Cu(111) effective potential from Ref. 64 and a wire-induced potential determined from DFT calculations. The choice of this construction procedure has several advantages. First, the splitting of the effective potential in two parts is physically transparent. It is well suited to study the properties of electronic excited states as has been shown, e.g., in the previous study on Cu adatoms.[42] In particular, it allows to get rid of the supercell geometry to study a single Cu chain and, thus, to efficiently describe the excited state decay (charge transfer between the Cu wire and the substrate). Second, the choice of a one-electron model potential for the clean Cu(111) surface allows us to easily include the correct image potential and surface/image state energies, which are not described in general by density-functional calculations based on local or semilocal exchange-correlation functionals, although more refined approaches can handle this problem.[78,79] Third, the full information about the wire-induced potential, which is one of the key ingredients in the present study, is retained from the density-functional calculations.

III. RESULTS AND DISCUSSION

A. Energy of the nanowire-localized 1D *sp*-band

Energetics of the system under the study is summarized in Fig. 2. The calculated energies of the 1D *sp*-band states are presented together with those of electronic states of the clean substrate. The system is periodic in z, the coordinate along the nanowire. In order to emphasize the dynamics and in

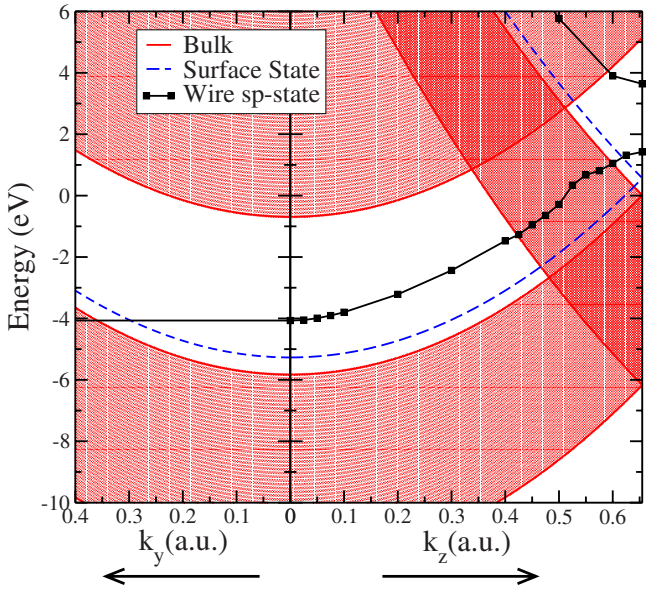

FIG. 2. (Color online) Electronic structure of the Cu nanowire on Cu(111) system as a function of the electron momentum parallel to the surface. The figure presents the substrate states: Shockley surface state (dashed blue line) and 3D propagating bulk states as well as the 1D *sp*-band states localized on the nanowire (black squares and full black line). The energies are shown with respect to the vacuum level. The left part of the figure shows the energy as a function of k_y (the electron momentum parallel to the surface and perpendicular to the wire) for $k_z=0$ (k_z is the electron momentum along the wire). The right part of the figure shows the energy as a function of k_z. The substrate states are shown for $k_y=0$ in the right panel.

particular the decay of the quasistationary states, we present a double figure showing the energy of the various states in the problem, as functions of k_y and k_z, the electron momentum projections on the two axes parallel to the surface. Because of the symmetry, only the energies corresponding to the positive wave-vector values are shown.

Two sets of electronic states of the clean Cu surface appear in the figures:

(i) The propagating 3D bulk states of the clean substrate have the following energy dispersion:

$$E_{3D}(k_x,k_y,k_z) = E(k_x) + k_y^2/2 + k_z^2/2. \tag{18}$$

$E(k_x)$ is the eigenenergy of the Bloch wave in the $V_S(x)$ model potential used here[64] and thus contains the information on the Cu band structure in the ΓL direction. Within the model potential,[64] the motion parallel to the surface is free-electron like. In the left panel of Fig. 2, the energy of the bulk states $E_{3D}(k_x,k_y,k_z)$ is shown for $k_z=0$, and in the right panel of Fig. 2 for $k_y=0$. The hatched area represents the k_x continuum of electronic states. Note the surface-projected band gap between −5.83 eV and −0.69 eV for $k_y=0$ and $k_z=0$.

(ii) The 2D Shockley-type surface state corresponds to an electron located at and propagating along the surface.[80] Its energy is inside the projected band gap of the substrate, and it is given by

$$E_{2D}(k_y,k_z) = E_S + k_y^2/2 + k_z^2/2, \tag{19}$$

with $E_S=-5.27$ eV.

The nanowire localized 1D *sp*-band appears inside the projected band gap of Cu(111). The *sp*-band states are localized in the *y* direction and so they do not disperse with k_y; the *sp*-band is thus shown as a straight line in the left panel of Fig. 2. In the right panel of Fig. 2, the calculated energies E_{1D} of the 1D *sp*-band states are shown as function of k_z, the electron wave vector along the nanowire. The energy dispersion appears basically parabolic. Fitting the calculated energies in the low k_z region with

$$E_{1D}(k_z) = E_W + k_z^2/2m^* \tag{20}$$

gives $E_W=-4.07$ eV and $m^*=0.5$, i.e., 50% of the free electron mass. The 0.5 value is quite close to the effective mass of the Cu(111) surface state, for which $m^*=0.412$ has been reported from photoemission studies.[81] This 1D dispersion is thus consistent with electron jumps along the Cu chain with a Cu-Cu distance equal to that in bulk Cu. An effective mass smaller than 1 has been also observed experimentally for different supported metallic wires.[31,32,34,37,82]

Now let us turn to a specific feature linked with the periodicity of the system in the *z* direction (right panel of Fig. 2). At the 1D Brillouin zone boundary ($k_z=\pm\mathcal{G}/2$), the 1D *sp*-band splits into a lower and an upper branch with a band gap of ~2 eV. The width of the lower energy subband is ~5.5 eV. This behavior is typical of a nearly free-electron system. The substrate electronic bands (3D bulk band states and the surface state) are backfolded at $k_z=\pm\mathcal{G}/2$, however, without band gap opening. Indeed, the continuum of substrate states is not modified by the presence of a single nanowire. The band backfolding appears as a result of mathematical constraint where, with periodic boundary conditions, one can choose between extended ($-\infty \le K_z \le +\infty$) or reduced ($-\mathcal{G}/2 \le k_z \le +\mathcal{G}/2$) band-structure representations. The upper branch of the folded bulk band in the figure corresponds to the $K_z=k_z-\mathcal{G}$ states of the extended band structure ($K_z \le -\mathcal{G}/2$). The corresponding energy relation is given by

$$E_{3D}(k_x,k_y,K_z) = E(k_x) + k_y^2/2 + (k_z-\mathcal{G})^2/2. \tag{21}$$

The band backfolding effect tends to partially close the projected band gap of the substrate or at least to partially soften its effect (see a more precise discussion below). The nanowire-localized 1D *sp*-band states appear in resonance with ($k_y=0$, $K_z=k_z-\mathcal{G}$) states of the 3D bulk for some values of k_z (crossing between the 1D *sp*-band dispersion curve and the states of the folded 3D band in the right panel of Fig. 2). The presence of the projected band gap and 3D band backfolding have very strong effects on the lifetimes of the nanowire-localized states as discussed below. At this point, one can also stress that, in the present work using the model potential representation of the Cu(111) substrate from,[64] the dispersion of the substrate states parallel to the surface corresponds to a free-electron motion and not to the proper effective mass. As a consequence, the actual k_z region where the band backfolding influences the system dynamics might be different from the one found here.

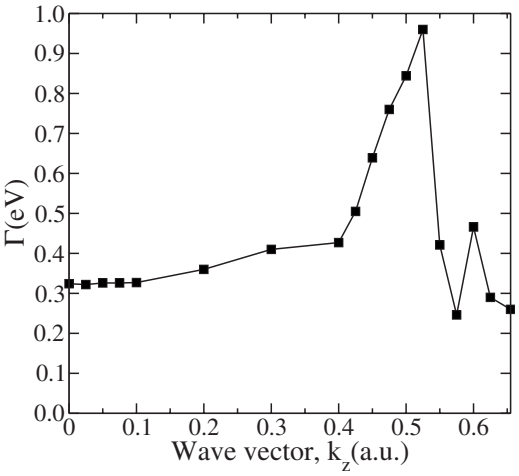

FIG. 3. Decay rate of the resonant *sp* state localized on a Cu wire supported on a Cu(111) surface as a function of the wave vector parallel to the wire, k_z.

B. Decay of the nanowire localized 1D *sp*-band states

The calculated resonant charge transfer (RCT) decay rate Γ of the nanowire localized states is presented in Fig. 3 as a function of the electron wave vector parallel to the wire k_z. Several ranges of k_z values can be observed on the figure with distinctly different $\Gamma(k_z)$ behavior. For k_z up to ~ 0.4 a.u., the RCT decay rate shows only a small variation between 0.3 and 0.4 eV. For $0.4 \leq k_z \leq 0.65$ a.u., $\Gamma(k_z)$ presents a sharp variation with a strong rise up to around 1 eV at $k_z \sim 0.525$ a.u. and then a fast drop followed by an additional structure around $k_z \sim 0.6$ a.u. These features in the $\Gamma(k_z)$ dependence can be understood from Fig. 2 showing the energies of the different states.

In the resonant charge transfer process, the initial 1D *sp*-band state of energy $E_{1D}(k_z)$ decays to substrate states with the same energy: either 3D propagating bulk states or the 2D surface state. Because of the periodicity, k_z, the electron wave vector along the nanowire is conserved or can change by an integer number of reciprocal lattice vectors, $n\mathcal{G}$ (the integer n denotes the diffraction order). From Eqs. (18) and (19) we then obtain

$$E_{1D}(k_z) = E(k_x) + k_y^2/2 + (k_z + n\mathcal{G})^2/2,$$

$$E_{1D}(k_z) = E_S + k_y^2/2 + (k_z + n'\mathcal{G})^2/2. \quad (22)$$

Thus, the energy resonance between the backfolded substrate states and the 1D *sp*-band states reflects the situation when the decay of the quasistationary nanowire-localized state is associated with a reciprocal lattice vector exchange (diffraction on the periodic structure).

As seen in the right panel of Fig. 2, for $k_z < 0.4$ a.u., the *sp*-band is inside the projected band gap of the substrate. There are no final states with $k_y = 0$ available for the electron escape from the nanowire. From the left panel of Fig. 2, or similarly from Eq. (22), it follows that RCT is only possible into the electronic states of the substrate with a finite k_y. These are the surface state with a fixed k_y and the bulk states with k_y above a certain value. Thus, because of the projected band gap, an electron escapes from the nanowire in the (xy) plane (see Fig. 1) beyond a certain angle away from the surface normal. The projected band gap thus blocks RCT along the surface normal, which is the direction of the lowest and shortest potential barrier between the nanowire and the substrate. One can *a priori* conclude that the 1D *sp*-band states are stabilized, and we assign the calculated width of $0.3 \div 0.4$ eV to the projected band-gap effect. Similar findings have been reported for single adatoms[42,57–61] and atomic projectiles.[65,83] The stabilizing effect of the surface-projected band gap is further stressed below by the analysis of the decay rates in the $0.4 < k_z < 0.6$ a.u. region.

For $0.4 < k_z < 0.6$ a.u., the nanowire-localized 1D *sp*-band (see Fig. 2) is in energy resonance with the backfolded substrate states with a wave vector $K_z = k_z - \mathcal{G}$, i.e., corresponding to the exchange of one reciprocal lattice vector, $n=-1$ in Eq. (22). Thus, a new RCT decay channel opens. Assisted by a reciprocal lattice vector exchange along the nanowire direction, an electron can escape from the nanowire into the substrate for $k_y = 0$. The projected band-gap effect is thus reduced, leading to a sizeable change in the decay rate Γ. Starting from $k_z = 0.4$ a.u., Γ grows, reflecting the energy resonance with folded 3D bulk band states further away from the band bottom. The decay rate reaches its maximum value for $k_z \approx 0.525$ a.u., and then it decreases again because the 1D *sp*-band is approaching the folded band gap.

There is an additional structure in $\Gamma(k_z)$ around 0.6 a.u. We did not study it in detail, but we can notice that, in this k_z range, the 1D *sp*-band is in energy resonance with the backfolded surface state band for $k_y = 0$ (see also Fig. 2). In this region, the RCT decay into the 2D surface state band with $k_y = 0$ becomes possible, when assisted by a reciprocal lattice vector exchange [$n=-1$ in Eq. (22)] and leads to the observed structure.

Thus, the lifetime of the 1D *sp*-band strongly depends on its energy with respect to the projected band gap of the substrate, and thus on k_z through the energy dispersion. The projected band gap leads to the stabilization of the nanowire-localized states (a longer lifetime), while the backfolding of the substrate bands at the Brillouin zone boundary brings additional decay channels and tends to increase the RCT decay rate. A similar effect of the substrate band backfolding has been reported recently for the 2D quantum well states in $p(2\times 2)$ Cs and Na ordered overlayers on Cu(111).[63,84,85]

The results obtained for the lifetime of the upper branch of the *sp*-band are consistent with the previous reasoning: in the k_z region in which the upper *sp*-band is located inside the projected band gap (see Fig. 2) it presents a decay rate of $\Gamma \sim 0.3$ eV. Γ rises to 0.7 eV when the upper *sp*-band is degenerated with 3D bulk states with $k_y \sim 0$.

The computed decay rate of the 1D *sp*-band corresponds to the one-electron energy-conserving resonant electron transfer (RCT) from the nanowire into the substrate states. However, the many-body energy relaxation also contributes to the decay of excited states at surfaces associated with adatoms,[56,59] or artificial structures on surfaces.[84,86] It corresponds to the interaction between the nanowire-localized electron and many-body substrate excitations with subsequent energy sharing between them.[56,87] On a free-electron metal substrate, the RCT is the dominating decay channel

and its rate Γ is at least 1 order of magnitude faster than the many-body energy relaxation rate Γ_{ee}. However, because of the RCT blocking by the projected band gap, the two channels may become comparable in efficiency so that the lifetime of the excited state is given by $\tau=1(\Gamma+\Gamma_{ee})$.[56,59] The calculation of the many-body decay rate of the nanowire-localized states was not attempted here. Rather, we estimated Γ_{ee} from previously measured and calculated data for different excited states at surfaces. For the alkali adsorbates on Cu(111), the rate of the many-body inelastic decay for the alkali-localized *sp* state was computed to be in the 20 meV range.[59,88] For extended states, such as quantum well states or states confined in quantum corrals, Γ_{ee} well below 20 meV have been reported[56,63,86] for states in the same energy range as the present 1D *sp*-band. Thus, it appears reasonable to assume that the many-body mechanisms are not significant in the present system since the typical Γ_{ee} rates are much smaller than the one-electron decay rate obtained for the 1D *sp*-band in this work ($\Gamma \sim 0.2-1.0$ eV). The lifetime of the 1D *sp*-band states can be then well approximated as $\tau=1/\Gamma$.

C. Wave functions

The different aspects of the decay of the nanowire-localized quasistationary states can be visualized on their wave functions. We have plotted in Fig. 4 the resonant wave function in the (xy) plane and in the (xz) plane for the ($k_z=0$) case [panels (a) and (b)], and for the ($k_z=0.5$) case [panels (c) and (d)]. In the first case, the 1D *sp*-band is inside the surface-projected band gap, and in the second case, the 1D *sp*-band is in the energy region of the backfolded bulk band states.

As a first observation, in both cases ($k_z=0$ and $k_z=0.5$ a.u.), the 1D nanowire localized state presents the typical characteristics of a delocalized state formed by the interaction between the sp_x hybrids localized on the Cu atoms of the nanowire. In the single adatom case, the long-lived sp_x hybrid is formed by the *s* and p_x atomic orbitals, and it is polarized along the surface normal away from the surface.[40–42] In Fig. 4, the 1D nanowire-localized state clearly shows two features: the delocalization of the excited electron density along the Cu atom chain and an electron density shifted from the geometrical center of the nanowire into the vacuum. This is very similar to previous studies of finite-size Cu monoatomic chains on Cu(111),[34,35] Au monoatomic chains on NiAl(110),[41] and Ag monoatomic chains on Ag(111) (Ref. 40) surfaces.

The different decays of the quasistationary states for $k_z=0$ and $k_z=0.5$ a.u. lead to very different behaviors inside the metal. Indeed, for $k_z=0$, the decay of the nanowire-localized 1D *sp*-band state appears in the (xy) plane as two symmetric outgoing fluxes inside the metal [panel (a)]. The finite angle between the outgoing electron flux and the surface normal is consistent with the projected band-gap effect: the nanowire-localized state is in resonance with metal continuum states only for some finite values of k_y (see Fig. 2). For $k_y=0$, the electron transfer is blocked by the projected band gap of the substrate and so, the electron density in the

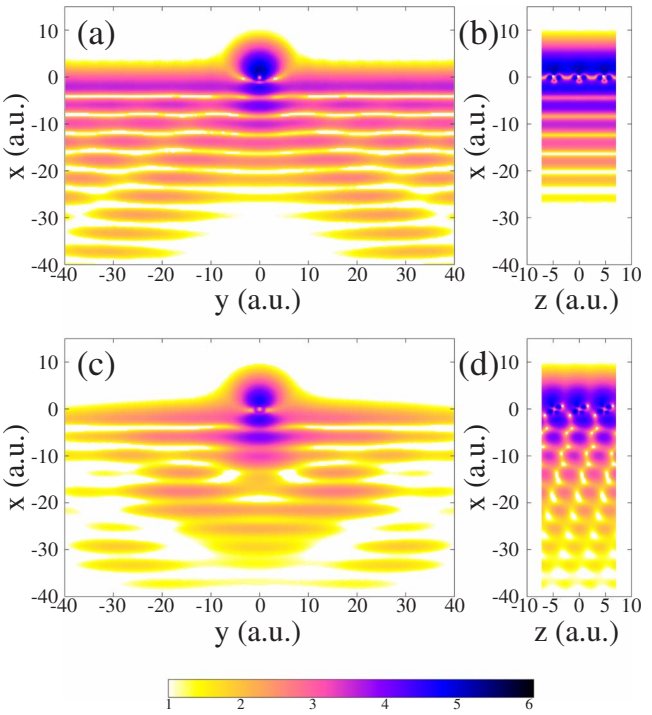

FIG. 4. (Color online) Electron density of the quasistationary *sp* state localized on a Cu nanowire supported on Cu(111). The figure presents the logarithm of the electron density for [(a) and (b)] $k_z=0$ and [(c) and (d)] $k_z=0.5$ a.u.. Results are shown in the (xy) and (xz) planes and the origin of coordinates is placed at one Cu atom of the wire (see Fig. 1). The dark areas correspond to a large probability of presence of the electron and the color code is given in the inset.

(xz) plane decays exponentially into the metal along the *x* axis [panel (b)]. The decay of the nanowire-localized state into the 2D continuum of the Cu(111) surface state appears in the panel (a) of the figure as an outgoing flux parallel to the surface around $x=-2$ a.u.. Observe that it is much more intense than the decay into the bulk metal leading to the conclusion that the surface state is the main decay channel for the nanowire-localized 1D *sp*-band states at low k_z.

For $k_z=0.5$ a.u., an additional decay channel is open. As already discussed, it consists in the electron escape from the nanowire into the metal continuum states characterized by $k_y=0$, and $k_z-\mathcal{G}$. It is seen in Fig. 2 as the resonance between the nanowire 1D *sp*-band dispersion curve and the backfolded substrate states. This "diffractive" decay is clearly seen in Fig. 4(d) where an outgoing flux into the metal appears along the negative direction of the *z* axis. In addition, in contrast to Fig. 4(a), in the panel (c) there is an outgoing flux from the nanowire into the metal along the surface normal. The interference pattern seen in Fig. 4(c) and in particular Fig. 4(d) reflects the coexistence of both the "diffractive" decay with $k_y=0$ and a reciprocal lattice vector exchange and the direct decay populating substrate states with a finite k_y [same as in Fig. 4(a)]. The decay into the surface state is much less pronounced in the $k_z=0.5$ a.u. case and the main decay is into bulk states.

Examining the resonance wave functions illustrates well the way the band folding softens the effect of the projected

band gap. In particular, it appears that the band folding is not really closing the surface-projected band gap. In the two decay modes illustrated in Fig. 4, the RCT process is not associated with an electron escaping along the surface normal; this is always forbidden by the surface-projected band gap. In both cases, the electron escapes a certain angle from the surface normal: either via a finite k_y value in the low k_z range or via a "diffractive" process ($K_z=k_z-\mathcal{G}$, possibly with $k_y=0$) in the $0.4<k_z<0.6$ a.u. range.

Thus, analysis of the wave functions of the quasistationary states appears quite helpful and illustrative in revealing different aspects of the RCT decay of the nanowire-localized 1D *sp*-band states: (i) effect of the projected band gap reducing the RCT efficiency; (ii) existence of two decay channels associated with electron transfer into the Cu(111) surface state continuum and into the 3D propagating bulk states; (iii) existence of a RCT decay process assisted by a reciprocal lattice vector exchange (band backfolding).

D. Distance traveled by excited electrons

The discussion of the excited electron dynamics in the Cu-wire/Cu(111) system and the role of the projected band gap can be completed with an estimate of the mean distance d traveled by an excited electron along the nanowire. From the energies $E(k_z)$ and lifetimes $\Gamma(k_z)$ of the 1D *sp*-band states, the mean distance d traveled by an excited electron before it escapes into the substrate can be obtained as

$$d(k_z) = \frac{\partial E(k_z)}{\partial k_z}\frac{1}{\Gamma(k_z)}, \tag{23}$$

where $v_g=\partial E(k_z)/\partial k_z$ is the group velocity, and $\tau=1/\Gamma(k_z)$ is the excited state lifetime.

The results had been presented in Fig. 5 of Ref. 62. Basically, starting from $k_z=0$ the distance d increases up to $k_z\sim 0.4$ a.u. In this k_z range, the 1D *sp*-band is inside the projected band gap, the RCT decay rate of the nanowire-localized states is almost constant (see Fig. 3), and d merely reflects the k_z dependence of the group velocity. The maximum propagation distance is $d\sim 12$ Å. Thus, thanks to the surface projected band gap of Cu(111), an electron injected into the *sp*-band of the nanowire-localized states can travel over four to five nanowire atoms before it escapes into the surface state or into the bulk. For higher values of the parallel momentum, the additional decay channel associated with a reciprocal lattice vector exchange opens and the travel distance d drops because of the decrease in the lifetime of the nanowire-localized state.

E. Comparison with STM experiments

In order to have a direct comparison with earlier scanning tunneling spectroscopy (STS) measurements,[34] the perturbation induced by the STM tip has to be included.[62] To this purpose, we have added an additional term, U_{STM}, to the total potential in Eq. (5). It was introduced assuming a simple planar capacitor model in which the potential in the STM junction increases linearly with the distance to the surface (x),

$$U_{\mathrm{STM}} = \begin{cases} 0 & \text{if } x < x_{\mathrm{im}} \\ F(x-x_{\mathrm{im}}) & \text{if } x_{\mathrm{im}} < x < x_{\mathrm{tip}} \\ U_0 & \text{if } x > x_{\mathrm{tip}}, \end{cases} \tag{24}$$

where x_{im} and x_{tip} are the surface image plane and tip apex positions, respectively. The slope (the field) is calculated as $F=U_0/(x_{\mathrm{tip}}-x_{\mathrm{im}})$ where U_0 is the applied voltage (bias). Following the experimental conditions,[34] we used in the simulations $x_{\mathrm{tip}}=7.42$ Å, i.e., 5.5 Å with respect to the center of the atomic wire. One can notice that since excited states above the Fermi level are probed, the potential due to the STM tip is repulsive and lifts the energies of the states. Actually, it appears that the energy of a quasistationary state under the STM tip, $E_{\mathrm{Field}}(U_0)$, shifts by a quantity roughly equal to a fraction of the STM bias, U_0:

$$E_{\mathrm{Field}}(U_0) \sim E_0 + \alpha U_0, \tag{25}$$

where E_0 is the state energy in the absence of the STM tip, i.e., the energy discussed in the previous sections. The coefficient α corresponds to the average position of the excited electron inside the capacitor. We then look iteratively for the value of the bias U_0 such that the quasistationary state energy $E_{\mathrm{Field}}(U_0)$ becomes equal to the bias, U_0. This yields the apparent energy, E_{app}, of the quasistationary state in the STS experiment.

The widths of the quasistationary states are also modified by the presence of the STM field. Two effects play a role:

(i) the applied field brings an extra force pulling the excited electron toward the surface leading to an increase in the decay rate of the state;

(ii) in an STS experiment, the energy spectrum is obtained by scanning the STM bias. As U_0 is scanned, the energy of the quasistationary states varies as discussed above. The shift of the resonance energy as the bias is scanned through the resonance profile makes the resonance look broader. To illustrate this point, we can use the approximate Eq. (25). The resonance center appears at the bias $U_0=E_0/(1-\alpha)$. In a field-free case, the two points defining the width of the resonance profile appear at $E_0-\Gamma/2$ and $E_0+\Gamma/2$. With the present effect of the scanning bias, they appear at $(E_0-\Gamma/2)/(1-\alpha)$ and $(E_0+\Gamma/2)(1-\alpha)$, leading to an apparent width equal to $\Gamma/(1-\alpha)$.

Figure 5 presents a comparison of experimental STS measurements[34,62] with computed results obtained including the STM bias effect. The apparent resonance energy with respect to the Fermi level, E_{app}, and the apparent width, Γ_{app}, of the 1D *sp* state are shown as a function of the wave vector parallel to the wire (k_z). An increase in the energy and width with respect to the results obtained in the field-free case is observed. It is indeed the consequence of the electric field in the STM junction and these results confirm the significant perturbing role of an STM probe. The figure also shows that our calculated results (both for the energy and width of the 1D *sp* state) are in very good agreement with the experimental measurements.[34,62] It thus gives us confidence in the set of computational methods used here.

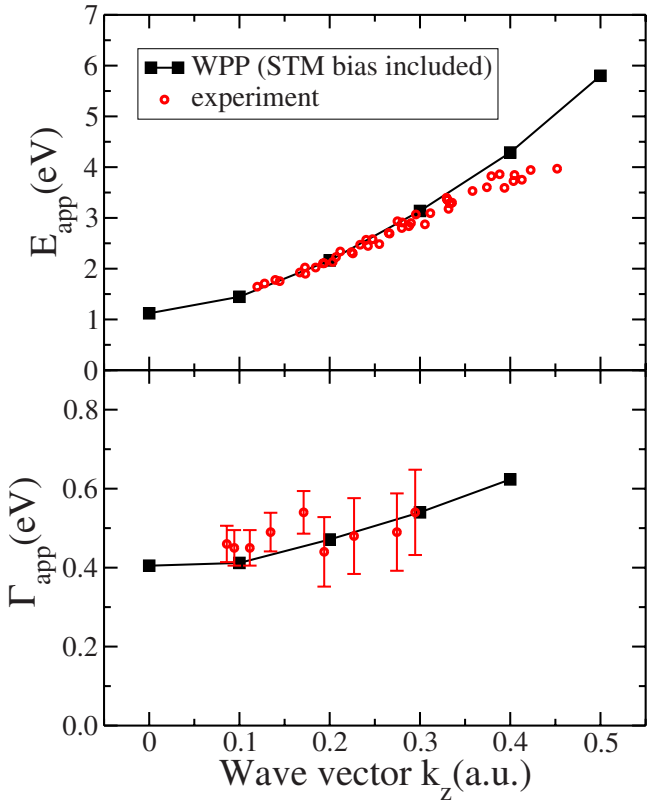

FIG. 5. (Color online) Energy with respect to the Fermi level (upper part) and width (lower part) of the *sp* state as a function of the wave vector parallel to the wire, k_z. Squares: Theoretical calculations with the effect of the STM bias included in the simulations; circles: experimental STS measurements (Refs. 34 and 62).

IV. CONCLUSIONS

We have performed a theoretical study of the excited electron dynamics in infinite Cu monoatomic chains (nanowires) supported on a Cu(111) surface. The system is an infinite analog of the finite-size chains studied recently with scanning tunneling microscope manipulation at surfaces.[31–40] In the above references and in the following theoretical works,[34,40,41,43] it has been demonstrated that the electronic structure of Cu-chain/Cu(111) is characterized by a one-dimensional chain-localized electronic band of excited states with *sp* character.

The present contribution addresses *both* the energy and the lifetime of the chain-localized states. In this purpose, a mixed approach is used, in which the nanowire-induced potential is obtained from *ab initio* density-functional theory calculations, the Cu(111) surface is represented with a model potential, and the dynamics of the excited electron is studied with the wave packet propagation approach. This allows us to remove the artificial effect of the supercell periodicity inherent to DFT treatments, and to avoid the quantization of the continuum of the electronic states of the substrate induced by the finite-size computational box. The latter is crucial for a reliable calculation of the width (decay rate) of the nanowire-localized electronic states.

The same strategy has been already applied in our earlier study of Cu-chain/Cu(111),[62] however, the present contribution substantially extends the work of Ref. 62 in that the energy dispersion and the lifetime of the chain-localized 1D *sp*-band is determined in a broad range of k_z, the electron momenta along the wire. In particular, this allows us to reach the regime where the surface Brillouin zone backfolding reduces the stabilization of the 1D *sp*-band states by the projected band gap of the Cu(111). Thus, a complete analysis of the effect of the projected band gap in decoupling the nanowire from the substrate could be performed.

Our main results can be summarized as follows:

(1) For low k_z (≤ 0.4 a.u.), the projected band gap of the Cu(111) substrate efficiently decouples the chain-localized 1D *sp*-band states from the substrate. The resonant electron transfer rates from the chain into the substrate are then reduced, and an excited electron can travel along up to five Cu atoms in the chain before its decay. Thus, the monoatomic wire appears as a separate entity and not as a protruding part of the substrate.

(2) In the $0.4 < k_z < 0.6$ a.u. range, the 1D *sp*-band dispersion curve is in resonance with substrate electronic bands backfolded at the surface Brillouin zone boundary. An additional decay channel of the nanowire-localized states opens. It consists in the resonant electron transfer between the 1D *sp*-band states and substrate electronic states associated with the exchange of a reciprocal lattice vector of the nanowire. The opening of this "diffractive" decay channel reduces the stabilization effect of the projected band gap and leads to a strong reduction in the lifetime of the 1D *sp*-band states.

(3) The resonant wave functions of the 1D *sp*-band states were extracted from the WPP for different k_z values. The associated electron densities nicely illustrate the projected band gap and the surface Brillouin zone backfolding effects on the decay of the nanowire localized states. The analysis of the resonant wave function also showed that the 2D continuum of the intrinsic surface state of Cu(111) is one of the main decay channels for the nanowire localized states and even the dominant one at low k_z.

Finally, our results are in good agreement with STS measurements. We show, in addition, how the scanning tunneling spectroscopy perturbs the electronic states of the nanowire (STM as a perturbing probe).

ACKNOWLEDGMENT

S.D-T. gratefully acknowledges support from the Spanish Ministerio de Educación y Ciencia and from the RTRA "Triangle de la Physique." The authors acknowledge very helpful discussions with Stefan Fölsch.

*sergio.diaz-tendero@u-psud.fr

[1] F. J. Himpsel, J. E. Ortega, G. J. Mankey, and R. F. Willis, Adv. Phys. **47**, 511 (1998).

[2] H. F. Ding, V. S. Stepanyuk, P. A. Ignatiev, N. N. Negulyaev, L. Niebergall, M. Wasniowska, C. L. Gao, P. Bruno, and J. Kirschner, Phys. Rev. B **76**, 033409 (2007).

[3] N. Nilius, M. V. Ganduglia-Pirovano, V. Brázdová, M. Kulawik, J. Sauer, and H.-J. Freund, Phys. Rev. Lett. **100**, 096802 (2008).

[4] J. A. Stroscio and D. M. Eigler, Science **254**, 1319 (1991).

[5] H. Ohnishi, Y. Kondo, and K. Takayanagi, Nature (London) **395**, 780 (1998).

[6] L. Bartels, G. Meyer, and K. H. Rieder, Phys. Rev. Lett. **79**, 697 (1997).

[7] M. F. Crommie, C. P. Lutz, and D. M. Eigler, Science **262**, 218 (1993).

[8] E. J. Heller, M. F. Crommie, C. P. Lutz, and D. M. Eigler, Nature (London) **369**, 464 (1994).

[9] J. Kliewer, R. Berndt, and S. Crampin, Phys. Rev. Lett. **85**, 4936 (2000).

[10] H. C. Manoharan, C. P. Lutz, and D. M. Eigler, Nature (London) **403**, 512 (2000).

[11] K.-F. Braun and K.-H. Rieder, Phys. Rev. Lett. **88**, 096801 (2002).

[12] S. Crampin, M. H. Boon, and J. E. Inglesfield, Phys. Rev. Lett. **73**, 1015 (1994).

[13] S. Crampin and O. R. Bryant, Phys. Rev. B **54**, R17367 (1996).

[14] V. S. Stepanyuk, L. Niebergall, W. Hergert, and P. Bruno, Phys. Rev. Lett. **94**, 187201 (2005).

[15] H. K. Harbury and W. Porod, Phys. Rev. B **53**, 15455 (1996).

[16] G. A. Fiete and E. J. Heller, Rev. Mod. Phys. **75**, 933 (2003).

[17] V. Madhavan, W. Chen, T. Jamneala, M. F. Crommie, and N. S. Wingreen, Science **280**, 567 (1998).

[18] D. Porras, J. Fernandez-Rossier, and C. Tejedor, Phys. Rev. B **63**, 155406 (2001).

[19] J. Li, W. D. Schneider, R. Berndt, and S. Crampin, Phys. Rev. Lett. **80**, 3332 (1998).

[20] J. Li, W.-D. Schneider, S. Crampin, and R. Berndt, Surf. Sci. **422**, 95 (1999).

[21] S. Pons, P. Mallet, and J.-Y. Veuillen, Phys. Rev. B **64**, 193408 (2001).

[22] L. Diekhöner, M. A. Schneider, A. N. Baranov, V. S. Stepanyuk, P. Bruno, and K. Kern, Phys. Rev. Lett. **90**, 236801 (2003).

[23] F. Calleja, J. J. Hinarejos, A. L. Vázquez de Parga, and R. Miranda, Eur. Phys. J. B **40**, 415 (2004).

[24] J. P. Gauyacq and A. G. Borisov, Surf. Sci. **600**, 825 (2006).

[25] L. Niebergall, G. Rodary, H. F. Ding, D. Sander, V. S. Stepanyuk, P. Bruno, and J. Kirschner, Phys. Rev. B **74**, 195436 (2006).

[26] S. Díaz-Tendero, A. G. Borisov, and J. P. Gauyacq, Phys. Rev. B **76**, 155428 (2007).

[27] Ph. Avouris and I. W. Lyo, Science **264**, 942 (1994).

[28] J. E. Ortega, F. J. Himpsel, R. Haight, and D. R. Peale, Phys. Rev. B **49**, 13859 (1994).

[29] L. Bürgi, O. Jeandupeux, A. Hirstein, H. Brune, and K. Kern, Phys. Rev. Lett. **81**, 5370 (1998).

[30] X. Y. Wang, X. J. Shen, R. M. Osgood, R. Haight, and F. J. Himpsel, Phys. Rev. B **53**, 15738 (1996).

[31] N. Nilius, T. M. Wallis, and W. Ho, Science **297**, 1853 (2002).

[32] T. M. Wallis, N. Nilius, and W. Ho, Phys. Rev. Lett. **89**, 236802 (2002).

[33] N. Nilius, T. M. Wallis, and W. Ho, Phys. Rev. Lett. **90**, 186102 (2003).

[34] S. Fölsch, P. Hyldgaard, R. Koch, and K. H. Ploog, Phys. Rev. Lett. **92**, 056803 (2004).

[35] S. Fölsch, P. Hyldgaard, R. Koch, and K. H. Ploog, Physica E **24**, 111 (2004).

[36] N. Nilius, T. M. Wallis, and W. Ho, Appl. Phys. A: Mater. Sci. Process. **80**, 951 (2005).

[37] N. Nilius, T. M. Wallis, and W. Ho, J. Phys. Chem. B **109**, 20657 (2005).

[38] J. Lagoute, X. Liu, and S. Fölsch, Phys. Rev. B **74**, 125410 (2006).

[39] J. Lagoute, C. Nacci, and S. Fölsch, Phys. Rev. Lett. **98**, 146804 (2007).

[40] A. Sperl, J. Kröger, N. Néel, H. Jensen, R. Berndt, A. Franke, and E. Pehlke, Phys. Rev. B **77**, 085422 (2008).

[41] M. Persson, Phys. Rev. B **70**, 205420 (2004).

[42] F. E. Olsson, M. Persson, A. G. Borisov, J. P. Gauyacq, J. Lagoute, and S. Fölsch, Phys. Rev. Lett. **93**, 206803 (2004).

[43] V. S. Stepanyuk, A. N. Klavsyuk, L. Niebergall, and P. Bruno, Phys. Rev. B **72**, 153407 (2005).

[44] S. Díaz-Tendero, F. E. Olsson, A. G. Borisov, and J. P. Gauyacq, Phys. Rev. B **77**, 205403 (2008).

[45] A. I. Yanson, I. K. Yanson, and J. M. van Ruitenbeek, Nature (London) **400**, 144 (1999).

[46] A. Nitzan, Annu. Rev. Phys. Chem. **52**, 681 (2001).

[47] C. Joachim, J. K. Gimzewski, and A. Aviram, Nature (London) **408**, 541 (2000).

[48] A. Nitzan and M. A. Ratner, Science **300**, 1384 (2003).

[49] M. Di Ventra, S. T. Pantelides, and N. D. Lang, Phys. Rev. Lett. **84**, 979 (2000).

[50] C. A. Mirkin and M. A. Ratner, Annu. Rev. Phys. Chem. **43**, 719 (1992).

[51] F. Favier, E. C. Walter, M. P. Zach, T. Benter, and R. M. Renner, Science **293**, 2227 (2001).

[52] *Molecular Electronics-Science and Technology*, edited by A. Aviram, AIP Conf. Proc. No. 262 (AIP, New York, 1992).

[53] A. Nitzan, Annu. Rev. Phys. Chem. **52**, 681 (2001).

[54] For an overview of the field, see *Introducing Molecular Electronics*, Lecture Notes in Physics Vol. 680, edited by G. Cuniberti, G. Fagas, and K. Richter (Springer Verlag, Berlin, 2005) (and references therein).

[55] T. Kishi, H. Kasai, H. Nakanishi, W. A. Diño, and F. Komori, Surf. Sci. **566–568**, 1052 (2004).

[56] E. V. Chulkov, A. G. Borisov, J. G. Gauyacq, D. Sánchez-Portal, V. M. Silkin, V. P. Zhukov, and P. M. Echenique, Chem. Rev. **106**, 4160 (2006).

[57] J. P. Gauyacq, A. G. Borisov, and M. Bauer, Prog. Surf. Sci. **82**, 244 (2007).

[58] A. G. Borisov, A. K. Kazansky, and J. P. Gauyacq, Surf. Sci. **430**, 165 (1999).

[59] A. G. Borisov, J. P. Gauyacq, E. V. Chulkov, V. M. Silkin, and P. M. Echenique, Phys. Rev. B **65**, 235434 (2002).

[60] S. Ogawa, H. Nagano, and H. Petek, Phys. Rev. Lett. **82**, 1931 (1999).

[61] M. Bauer, S. Pawlik, and M. Aeschlimann, Phys. Rev. B **60**, 5016 (1999).

[62] S. Díaz-Tendero, S. Fölsch, F. E. Olsson, A. G. Borisov, and J. P. Gauyacq, Nano Lett. **8**, 2712 (2008).

[63] C. Corriol, V. M. Silkin, D. Sánchez-Portal, A. Arnau, E. V.

Chulkov, P. M. Echenique, T. von Hofe, J. Kliewer, J. Kröger, and R. Berndt, Phys. Rev. Lett. **95**, 176802 (2005).
[64] E. V. Chulkov, V. M. Silkin, and P. M. Echenique, Surf. Sci. **437**, 330 (1999).
[65] A. G. Borisov, A. K. Kazansky, and J. P. Gauyacq, Phys. Rev. B **59**, 10935 (1999).
[66] F. E. Olsson, A. G. Borisov, and J. P. Gauyacq, Surf. Sci. **600**, 2184 (2006).
[67] T. Hakala, M. J. Puska, A. G. Borisov, V. M. Silkin, N. Zabala, and E. V. Chulkov, Phys. Rev. B **75**, 165419 (2007).
[68] D. Neuhauser and M. Baer, J. Chem. Phys. **91**, 4651 (1989).
[69] M. D. Feit, J. A. Fleck, Jr., and A. Steiger, J. Comput. Phys. **47**, 412 (1982).
[70] M. D. Feit and J. A. Fleck, Jr., J. Chem. Phys. **78**, 301 (1983).
[71] R. Kosloff, J. Phys. Chem. **92**, 2087 (1988).
[72] R. Kosloff, Annu. Rev. Phys. Chem. **45**, 145 (1994).
[73] G. Kresse and J. Furthmüller, Phys. Rev. B **54**, 11169 (1996).
[74] L. Kleinman and D. M. Bylander, Phys. Rev. Lett. **48**, 1425 (1982).
[75] D. M. Ceperley and B. J. Alder, Phys. Rev. Lett. **45**, 566 (1980).
[76] J. P. Perdew and A. Zunger, Phys. Rev. B **23**, 5048 (1981).
[77] A. G. Borisov, J. P. Gauyacq, and S. V. Shabanov, Surf. Sci. **487**, 243 (2001).
[78] A. G. Eguiluz, M. Heinrichsmeier, A. Fleszar, and W. Hanke, Phys. Rev. Lett. **68**, 1359 (1992).
[79] V. M. Silkin, E. V. Chulkov, and P. M. Echenique, Phys. Rev. B **60**, 7820 (1999).
[80] M. C. Desjonquères and D. Spanjaard, *Concepts in Surface Physics*, Springer Series in Surface Sciences Vol. 30 (Springer-Verlag, Berlin, 1993).
[81] F. Reinert, G. Nicolay, S. Schmidt, D. Ehm, and S. Hüfner, Phys. Rev. B **63**, 115415 (2001).
[82] K. N. Altmann, J. N. Crain, A. Kirakosian, J. L. Lin, D. Y. Petrovykh, F. J. Himpsel, and R. Losio, Phys. Rev. B **64**, 035406 (2001).
[83] A. G. Borisov, A. K. Kazansky, and J. P. Gauyacq, Phys. Rev. Lett. **80**, 1996 (1998).
[84] J. Kröger, M. Becker, H. Jensen, Th. von Hofe, N. Néel, L. Limot, R. Berndt, S. Crampin, E. Pehlke, C. Corriol, V. M. Silkin, D. Sánchez-Portal, A. Arnau, E. V. Chulkov, and P. M. Echenique, Prog. Surf. Sci. **82**, 293 (2007).
[85] D. Sánchez-Portal, Prog. Surf. Sci. **82**, 313 (2007).
[86] S. Crampin, H. Jensen, J. Kröger, L. Limot, and R. Berndt, Phys. Rev. B **72**, 035443 (2005).
[87] P. M. Echenique, J. M. Pitarke, E. V. Chulkov, and A. Rubio, Chem. Phys. **251**, 1 (2000).
[88] A. G. Borisov, J. P. Gauyacq, A. K. Kazansky, E. V. Chulkov, V. M. Silkin, and P. M. Echenique, Phys. Rev. Lett. **86**, 488 (2001).